Monthly Notices
of the
ROYAL ASTRONOMICAL SOCIETY

MNRAS **449,** L11–L15 (2015) doi:10.1093/mnrasl/slu204

Astrochemistry at work in the L1157-B1 shock: acetaldehyde formation

C. Codella,[1⋆] F. Fontani,[1] C. Ceccarelli,[2,3] L. Podio,[1] S. Viti,[4] R. Bachiller,[5] M. Benedettini[6] and B. Lefloch[2,3]

[1]*INAF–Osservatorio Astrofisico di Arcetri, L.go E. Fermi 5, I-50125 Firenze, Italy*
[2]*Univ. Grenoble Alpes, IPAG, F-38000 Grenoble, France*
[3]*CNRS, IPAG, F-38000 Grenoble, France*
[4]*Department of Physics and Astronomy, University College London, Gower Street, London WC1E 6BT, UK*
[5]*IGN, Observatorio Astronómico Nacional, Calle Alfonso XIII, E-28004 Madrid, Spain*
[6]*INAF, Istituto di Astrofisica e Planetologia Spaziali, via Fosso del Cavaliere 100, I-00133 Roma, Italy*

Accepted 2014 December 23. Received 2014 December 22; in original form 2014 October 27

ABSTRACT

The formation of complex organic molecules (COMs) in protostellar environments is a hotly debated topic. In particular, the relative importance of the gas phase processes as compared to a direct formation of COMs on the dust grain surfaces is so far unknown. We report here the first high-resolution images of acetaldehyde (CH_3CHO) emission towards the chemically rich protostellar shock L1157-B1, obtained at 2 mm with the IRAM Plateau de Bure interferometer. Six blueshifted CH_3CHO lines with E_u = 26–35 K have been detected. The acetaldehyde spatial distribution follows the young ($\sim$ 2000 yr) outflow cavity produced by the impact of the jet with the ambient medium, indicating that this COM is closely associated with the region enriched by iced species evaporated from dust mantles and released into the gas phase. A high CH_3CHO relative abundance, 2–3 $\times$ 10^{-8}, is inferred, similarly to what found in hot corinos. Astrochemical modelling indicates that gas phase reactions can produce the observed quantity of acetaldehyde only if a large fraction of carbon, of the order of 0.1 per cent, is locked into iced hydrocarbons.

Key words: molecular data – stars: formation – ISM: molecules – radio lines: ISM – submillimetre: ISM.

1 INTRODUCTION

Complex organic molecules (COMs) have a key role among the many molecules so far detected in space: since they follow the same chemical rules of carbon-based chemistry, which terrestrial life is based on, they may give us an insight into the universality of life. Of course, large biotic molecules are not detectable in space, certainly not via (sub)millimetre observations. However, to determine whether pre-biotic molecules may form in space, we first need to understand the basic mechanisms that form smaller COMs. There is an extensive literature on the subject and still much debate on how COMs may form in space (e.g. Herbst & van Dishoeck 2009; Caselli & Ceccarelli 2012; Bergin 2013). Two basic processes are, in principle, possible: COMs may form on the grain surfaces or in gas phase. It is possible and even probable that the two processes are both important in different conditions for different molecules.

Acetaldehyde (CH_3CHO) has been detected in a large range of interstellar conditions and with different abundances, namely in hot cores (Blake et al. 1986), hot corinos (Cazaux et al. 2003), cold envelopes (Jaber et al. 2014), Galactic Centre clouds (Requena-Torres et al. 2006) and prestellar cores (Öberg et al. 2010). Grain surface models predict that CH_3CHO is one of the simplest COMs and can be formed either by the combination of two radicals on the grain surface, CH_3 and HCO, which become mobile when the grain temperature reaches $\sim$30 K (Garrod & Herbst 2006), or by irradiation of iced CH_4, CO_2 and other iced species (Bennett et al. 2005). For the former route, the two radicals are predicted to be formed either because of the photolysis of more complex molecules on the grain mantles or, more simply, because of the partial hydrogenation of simple biatomic molecules on the grain mantles (Taquet, Ceccarelli & Kahane 2012). Conversely, gas phase models claim that acetaldehyde is easily formed by the oxidation of hydrocarbons, which are produced by the hydrogenation of carbon chain on the grain mantles (Charnley, Tielens & Millar 1992; Charnley 2004). Finally, a further possible mechanism involving formation in the very high density gas phase immediately after ice mantles are sublimated has been proposed by Rawlings et al. (2013).

In general, it is very difficult to distinguish which of these three mechanisms are at work and, consequently, their relative importance. The chemically rich shocked region L1157-B1 offers a unique possibility to test these theories, as it is a place where the dust is not heated by the protostar, but some of the grain mantles are sputtered/injected in the gas phase because of the passage of a shock

⋆ E-mail: codella@arcetri.astro.it

Table 1. List of CH_3CHO transitions detected towards L1157-B1.

Transition	ν^a (GHz)	$E_u{}^a$ (K)	$S\mu^{2a}$ (D^2)	$\log(A/s^{-1})^a$
$(7_{0,7}–6_{0,6})$E	133.830	26	88.5	–4.04
$(7_{0,7}–6_{0,6})$A	133.854	26	88.4	–4.08
$(7_{2,6}–6_{2,5})$A	134.694	35	81.3	–4.11
$(7_{2,6}–6_{2,5})$E	134.895	35	79.7	–4.12
$(7_{2,5}–6_{2,4})$E	135.477	35	79.7	–4.11
$(7_{2,5}–6_{2,4})$A	135.685	35	81.3	–4.10

[a]From the Jet Propulsion Laboratory data base (Pickett et al. 1998).

(see e.g. Fontani et al. 2014). The L1157-mm protostar ($d = 250$ pc) drives a chemically rich outflow (Bachiller et al. 2001), associated with molecular clumpy cavities (Gueth, Guilloteau & Bachiller 1996), created by episodic events in a precessing jet. Located at the apex of the more recent cavity, the bright bow shock called B1 has a kinematical age of 2000 yr. This shock spot has been the target of several studies [e.g. the Large Programs Herschel/CHESS[1] (Chemical Herschel Surveys of Star forming regions; Ceccarelli et al. 2010; and IRAM-30m/ASAI[2] (Astrochemical Survey At IRAM]. In this Letter, we report high spatial resolution observations of acetaldehyde, with the aim to constrain and quantify the contribution of gas phase chemistry to the CH_3CHO formation.

2 OBSERVATIONS

L1157-B1 was observed with the IRAM Plateau de Bure (PdB) 6-element array in 2013 April–May using both the C and D configurations, with 21–176 m baselines, filtering out structures ≥20 arcsec, and providing an angular resolution of 2.5 arcsec × 2.3 arcsec (PA = 90°). The primary half-power beam width (HPBW) is ∼37 arcsec. The observed CH_3CHO lines (see Table 1) at ∼ 134–136 GHz were detected using the WideX backend which covers a 4-GHz spectral window at a 2-MHz (∼4.4 km s^{-1}) spectral resolution. The system temperature was 100–200 K in all tracks, and the amount of precipitable water vapour was generally ∼5 mm. Calibration was carried out following standard procedures, using GILDAS-CLIC.[3] Calibration was performed on 3C279 (bandpass), 1926+611 and 1928+738 (phase and amplitude). The absolute flux scale was set by observing MWC349 (∼1.5 Jy at 134 GHz). The typical rms noise in the 2 MHz channels was ∼0.7 mJy $beam^{-1}$.

3 RESULTS: IMAGES AND SPECTRA

Acetaldehyde emission has been clearly (S/N ≥ 10) detected towards L1157-B1. Fig. 1 shows the map of the $CH_3CHO(7_{0,7}–6_{0,6})$ E and A lines integrated emission. In order to verify whether the present CH_3CHO image is altered by filtering of large-scale emission, we produced the $CH_3CHO(7_{0,7}–6_{0,6})$ E+A spectrum summing the emission measured at PdBI in a circle of diameter equal to the HPBW of the IRAM-30m telescope (17 arcsec). We evaluated the missing flux by comparing such emission with the spectrum directly measured with the single dish (from the ASAI spectral survey, Lefloch et al., in preparation). As already found for

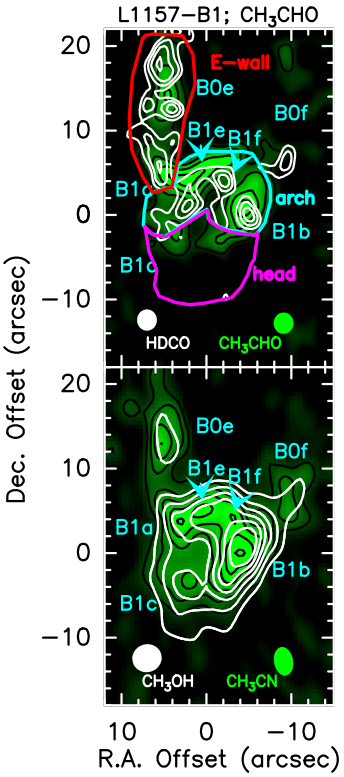

Figure 1. Chemical differentiation in L1157-B1: the maps are centred at $\alpha(J2000) = 20^h39^m09^s.5$, $\delta(J2000) = +68°01'10''.0$, i.e. at $\Delta\alpha = +21''.7$ and $\Delta\sigma = -64''.0$ from the driving protostar. Upper panel: $CH_3CHO(7_{0,7}–6_{0,6})$E+A integrated emission (green colour, black contours) on top of the $HDCO(2_{1,1}–1_{0,1})$ line (white contours; Fontani et al. 2014). First contour and steps of the CH_3CHO image corresponds to 3σ (1 mJy $beam^{-1}$). The ellipses show the synthesized HPBW (2.5 arcsec × 2.3 arcsec, PA = 90°). The red, turquoise and magenta polygons called 'E-wall', 'arch' and 'head' indicate the three portions of L1157-B1 selected by Fontani et al. (2014) to investigate H_2CO deuteration. Bottom panel: $CH_3CN(8_K–7_K)$ emission (green colour, black contours; Codella et al. 2009) on top of the $CH_3OH(3_2–2_K)$ emission (white; Benedettini et al. 2013). The HPBWs are 3.4 arcsec × 2.1 arcsec (PA = 10°) for CH_3CN and 3.5 arcsec × 2.3 arcsec (PA = 12°) for CH_3OH. The labels indicate the L1157-B1 clumps identified using the CH_3CN image (Codella et al. 2009).

HDCO by Fontani et al. (2014), with the PdBI we recover more than 80 per cent of the flux, indicating that both tracers do not have significant extended structures. The spatial distribution reported in Fig. 1 shows that CH_3CHO is mainly associated with two regions: (i) the eastern B0-B1 cavity opened by the precessing jet (called 'E-wall', see fig. 1 in Fontani et al. 2014), and (ii) the arch-like structure composed by the B1a-e-f-b clumps identified by CH_3CN (called 'arch'). The red, turquoise and magenta polygons shown in Fig. 1 sketch out these two regions, intersecting at the position of the B1a clump. Note that B1a is in turn located where the precessing jet is expected to impact the cavity producing a dissociative *J*-shock (traced by high velocity SiO, H_2O, [Fe II], [O I] and high-*J* CO emission: e.g. Gueth, Guilloteau & Bachiller 1998; Benedettini et al. 2012).

Fig. 2 shows the CH_3CHO line spectrum observed with the 3.6-GHz WideX bandwidth towards the brightest clump, B1a. Up to six lines (E_u = 26–35 K, see Table 1) are detected with an S/N > 3. Using the GILDAS–WEEDS package (Maret et al. 2011) and assuming optically thin emission and local thermodynamic equilibrium (LTE) conditions, we produced the synthetic spectrum (red line in Fig. 2)

[1] http://www-laog.obs.ujf-grenoble.fr/heberges/chess/
[2] http://www.oan.es/asai
[3] http://www.iram.fr/IRAMFR/GILDAS

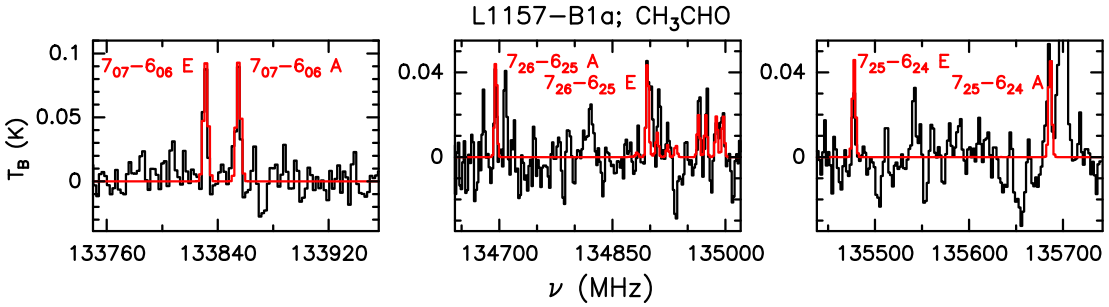

Figure 2. CH_3CHO emission (in T_B scale) extracted at the B1a position (α(J2000) = $20^h39^m10\overset{s}{.}2$, δ(J2000) = $+68°01'12\overset{''}{.}0$). The three panels show the frequency intervals of the 4-GHz-wide WideX where the six CH_3CHO lines with S/N $\geq 3\sigma$ (33 mK) are located (see Table 1). The red line shows the synthetic spectra which better reproduce the observations: it has been obtained with the GILDAS–WEEDS package (Maret et al. 2011) assuming optically thin emission and LTE conditions with $N_{CH_3CHO} = 9 \times 10^{13}$ cm^{-2}, $T_{ex} = 15$ K, $v_{LSR} = +0.6$ km s^{-1} and FWHM linewidth = 8.0 km s^{-1}.

Table 2. Observed parameters (in T_B scale) of the $CH_3CHO(7_{0,7}–6_{0,6})$E and A emission, and acetaldehyde column densities N_{CH_3CHO} derived in the three regions identified in Fig. 1 (E-wall, arch and head) following Fontani et al. (2014), see Section 3. The (range of) excitation temperatures (T_{ex}) used to derive N_{CH_3CHO} have been assumed equal to the rotation temperatures derived in Codella et al. (2012), Lefloch et al. (2012) and Fontani et al. (2014). The last columns report the $X(CH_3CHO)/X(CH_3OH)$ and $X(CH_3CHO)/X(HDCO)$ abundance ratios using the CH_3OH and HDCO data (and similar beams) by Benedettini et al. (2013) and Fontani et al. (2014).

Transition	T_{peak}[a] (mK)	V_{peak}[a] (km s^{-1})	FWHM[a] (km s^{-1})	F_{int}[a] (mK km s^{-1})	N_{CH_3CHO}[b] (10^{12} cm^{-2}) 10 K–70 K	CH_3CHO/CH_3OH (10^{-2}) 10 K–70 K	$CH_3CHO/HDCO$ 10 K–70 K
				E-wall			
$7_{0,7}–6_{0,6}$ E	30(3)	+0.4(0.4)	8.2(1.0)	264(28)			
					5.0(0.3)–9.2(0.5)	1.7(0.1)–11.0(0.6)	1.9(0.2)–0.9(0.1)
$7_{0,7}–6_{0,6}$ A	29(3)	+0.5(0.5)	8.6(1.3)	263(31)			
				Arch			
$7_{0,7}–6_{0,6}$ E	71(7)	–0.9(0.3)	9.2(0.8)	748(54)			
					15.9(0.1)–29.4(0.1)	0.6(0.1)–4.2(0.1)	7.6(1.1)–3.7(0.5)
$7_{0,7}–6_{0,6}$ A	76(7)	–0.2(0.9)	8.0(0.5)	608(42)			
				Head			
$7_{0,7}–6_{0,6}$ E	14(3)	+0.9(0.5)	8.0(1.1)	81(13)			
					1.7(0.3)–3.1(0.5)	0.2(0.1)–0.7(0.1)	≥ 1.5
$7_{0,7}–6_{0,6}$ A	13(3)	+0.9(0.6)	5.2(1.6)	81(13)			

[a]The errors are the Gaussian fit uncertainties. The spectral resolution is 4.4 km s^{-1}. [b]Derived using the $(7_{0,7}–6_{0,6})$ E and A emissions.

that best fits the observed one. Note that the CH_3CHO lines are blueshifted, by 2 km s^{-1}, with respect to the cloud systemic velocity (+2.6 km s^{-1}; Bachiller & Peréz Gutiérrez 1997), and have linewidths of 8 km s^{-1}. Similarly, we extracted the CH_3CHO line spectrum towards the three B1 zones, 'E-wall', 'arch' and 'head', shown in Fig. 1. Table 2 reports the measured peak velocities, intensities (in T_B scale), full width at half-maximum (FWHM) linewidths and integrated intensities, for each of the three zones.

4 CH_3CHO ABUNDANCE

Fig. 1 compares the CH_3CHO distribution with that of HDCO (Fontani et al. 2014), showing an excellent agreement, with weak or no emission at the head of the bow B1 structure (called 'head'). The acetaldehyde emission is concentrated towards the 'E-wall' and 'arch' zones, namely the part of B1 associated with the most recent shocked material, as probed by the HDCO emission. This is further supported by the fact that the brightest acetaldehyde emission comes where also CH_3OH, another dust mantle product, and CH_3CN, a 6-atom COM, emission peak (Codella et al. 2009; Benedettini et al. 2013). Finally, the CH_3CHO observed emission is also confined in the low-velocity range (FWHM $\sim$ 8 km s^{-1}) of the L1157-B1 outflow, which is dominated by the extended B1 bow-cavity, according to Lefloch et al. (2012) and Busquet et al. (2014). In summary, similarly to HDCO, CH_3CHO traces the extended interface between the shock and the ambient gas, which is chemically enriched by the sputtering of the dust mantles.

To derive the column density, we used the LTE populated and optically thin assumption and best fitted the six detected lines of Tables 1 and 2. Towards the B1a peak, we find $N_{CH_3CHO} = 9 \times 10^{13}$ cm^{-2}, and a rotational temperature of $T_{rot} = 15$ K, in agreement with the value derived for the molecular cavity from single-dish CO and HDCO measurements (10–70 K; Codella et al. 2012; Lefloch et al. 2012). Assuming rotational temperatures between 10 and 70 K (Table 2), we derived a column density of 5–30 $\times 10^{12}$ cm^{-2} in the 'E-wall' and 'arch' regions, and $\sim$2–3 10^{12} cm^{-2} in the 'head'. The size of the regions (at 3σ level) is 9 arcsec ('E-wall'), 7 arcsec ('arch') and 8 arcsec ('head'). An estimate of the CH_3CHO abundance can be derived using the CO column density $\simeq 10^{17}$ cm^{-2} derived by Lefloch et al. (2012) on a 20 arcsec scale. We derived N_{CH_3CHO} using the CH_3CHO spectrum extracted on the same scale and assuming 10–70 K. We find $N_{CH_3CHO} \sim 0.9–1.6 \times 10^{13}$ cm^{-2}, which implies a high abundance, $X(CH_3CHO) \simeq 2–3 \times 10^{-8}$, similar to what has been measured

in hot corinos ($\simeq$2–6 $\times$ 10^{-8}, Cazaux et al. 2003), and larger than that measured in prestellar cores ($\sim10^{-11}$; Vastel et al. 2014) and towards high-mass star forming regions ($\sim10^{-11}$–10^{-9}; Cazaux et al. 2003; Charnley 2004).

5 GAS PHASE FORMATION OF CH_3CHO

The ratio between N_{CH_3CHO} and the column density of HDCO, i.e. a molecule which in L1157-B1 is predominantly released by grain mantles (Fontani et al. 2014), is higher (even if we consider the uncertainties, see Table 2) in the 'arch' with respect to the 'E-wall' by a factor $\sim$2–8. Assuming the same grain mantle composition and release mechanism, this difference suggests that, in the 'arch', a significative fraction of the observed CH_3CHO is formed in the gas phase. In the gas phase, the injection from grain mantles of ethane (C_2H_6) is expected to drive first C_2H_5 and successively acetaldehyde (e.g. Charnley 2004; Vasyunin & Herbst 2013): the overlap between the HDCO (Fontani et al. 2014) and CH_3CHO emitting regions supports this scenario. We can, therefore, use the measured CH_3CHO abundance to constrain the quantity of C_2H_5 that has to be present in the gas phase in order to produce the observed quantity of CH_3CHO. To this end, we use the chemical code ASTROCHEM,[4] a pseudo-time-dependent model that follows the evolution of a gas cloud with a fixed temperature and density considering a network of chemical reactions in the gas phase. We followed the same two-step procedure adopted in Podio et al. (2014) and Mendoza et al. (2014), to first compute the steady-state abundances in the cloud (i.e. T_{kin} = 10 K, n_{H_2} = 10^4 cm^{-3}, ζ = 3 10^{16} s^{-1}); and then we follow the gas evolution over 2000 yr at the shocked conditions (i.e. T_{kin} = 70 K and n_{H_2} = 10^5 cm^{-3}). To estimate the influence of a possibly larger gas T_{kin} during the passage of the shock, we also run cases with temperatures up to 1000 K. We adopt the OSU[5] chemical network and assume visual extinction of A_V = 10 mag and grain size of 0.1 μm. We assume that the abundances of OCS and CO_2 are also enhanced by the passage of the shock, namely their abundance in step 2 is $X(CO_2) = 6 \times 10^{-5}$ and $X(OCS) = 6 \times 10^{-6}$. Similarly, we assume that the abundance of methanol in step 2 is 2 $\times$ 10^{-6}, in agreement with the most recent determination in L1157-B1 by Mendoza et al. (2014). Finally, we varied the C_2H_5 abundance from 2 $\times$ 10^{-7} to 2 $\times$ 10^{-5}. As expected, the predicted steady-state abundance of acetaldehyde in the cloud is very low (1.5 $\times$ 10^{-15}). However, once C_2H_5 is in the gas phase, it rapidly reacts with oxygen forming abundant acetaldehyde on time-scale shorter than 100 yr (Fig. 3). The CH_3CHO abundance reaches the observed value, $\simeq$2–3 $\times$ 10^{-8}, at the shock age (2000 years), for C_2H_5 $\sim$ 2–6 $\times$ 10^{-7}. Note that we obtain the same result if the gas temperature is $\leq$500 K, and a 30 per cent higher value at 1000 K. Fig. 3 shows also that the CH_3CHO/CH_3OH abundance ratio is expected to drop between 10^3 and 10^4 yr. A different age could, therefore, justify the slightly smaller CH_3CHO/CH_3OH ratio observed towards the 'head' region.

6 DISCUSSION AND CONCLUSIONS

We have shown that acetaldehyde is abundant, $X(CH_3CHO) \simeq$ 2–3 $\times$ 10^{-8}, in the gas associated with the passage of a shock and enriched by iced species sputtered from grain mantles and injected into the gas phase. The measured acetaldehyde abundance could be consistent with the scenario of oxidation of gaseous hydrocarbons formed in a previous phase and released by the grain mantles. However, the abundance of the C_2H_5 required to reproduce the measured CH_3CHO is very high, $\sim$2–6 $\times$ 10^{-7}, namely less than 0.6 per cent the elemental gaseous carbon. There are no observations of C_2H_5, hence it is impossible to compare with direct estimates of the abundance of this molecule. However, it has been argued that large quantities of frozen methane, of a few per cent of iced mantle water, is found around the L1527-mm protostar, where the detection of CH_3D (Sakai et al. 2012) indicates $X(CH_4) \simeq$ 0.4–1.5 $\times$ 10^{-5}. This large abundance has been attributed to a low density of the pre-collapse core from which L1527-mm originated (Aikawa et al. 2008). Interestingly, the analysis of the deuteration of water, methanol and formaldehyde in L1157-B1 led Codella et al. (2012) to conclude that also the mantles of L1157-B1 were formed in relatively low density ($\sim10^3$ cm^{-3}) conditions.

To conclude, in the specific case of L1157-B1, gas phase reactions can produce the observed quantity of acetaldehyde only if a large fraction of carbon, of the order of 0.1 per cent, is locked into iced hydrocarbons. Further observations of the hydrocarbons abundance in L1557-B1 are needed to confirm or dismiss our hypothesis.

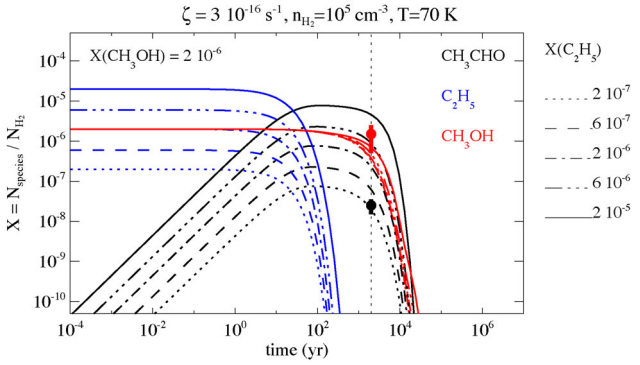

Figure 3. Evolution of acetaldehyde (CH_3CHO, black), (C_2H_5, blue) and methanol (CH_3OH, red) abundances in the shock as a function of time. Observed abundances (colour circles) are overplotted at the shock age (t_{shock} $\sim$ 2000 yr, vertical dotted line). The evolution is computed from steady-state values in the cloud (n_{H_2} = 10^4 cm^{-3}, T_{kin} = 10 K, ζ = 3 $\times$ 10^{-16} s^{-1}) by enhancing the gas temperature and density (n_{H_2} = 10^5 cm^{-3}, T_{kin} = 70 K), and the abundance of molecules which are thought to be sputtered off dust grain mantles. We set X_{CO_2} = 6 $\times$ 10^{-5} and X_{OCS} = 6 $\times$ 10^{-6} as in Podio et al. (2014), X_{CH_3OH} = 2 $\times$ 10^{-6} (Mendoza et al. 2014), and vary the abundance of C_2H_5 between 2 $\times$ 10^{-7} and 2 $\times$ 10^{-5}.

ACKNOWLEDGEMENTS

The authors are grateful to P. Caselli for instructive comments and suggestions, as well as to the IRAM staff for its help in the calibration of the PdBI data. This research has received funding from the European Commission Seventh Framework Programme (FP/2007-2013, no. 283393, RadioNet3), the PRIN INAF 2012 – JEDI and the Italian Ministero dell'Istruzione, Università e Ricerca through the grant Progetti Premiali 2012 – iALMA. LP has received funding from the European Union Seventh Framework Programme (FP7/2007-2013, n. 267251). CC and BL acknowledge the financial support from the French Space Agency CNES, and RB from Spanish MINECO (FIS2012-32096).

[4] http://smaret.github.com/astrochem/
[5] http://faculty.virginia.edu/ericherb

REFERENCES

Aikawa Y., Wakelam V., Garrod R. T., Herbst E., 2008, ApJ, 674, 993
Bachiller R., Peréz Gutiérrez M., 1997, ApJ, 487, L93
Bachiller R., Pérez Gutiérrez M., Kumar M. S. N., Tafalla M., 2001, A&A, 372, 899
Benedettini M. et al., 2012, A&A, 539, L3
Benedettini M. et al., 2013, MNRAS, 436, 179
Bennett C. J., Osamira Y., Lebar M. D., KAiser R. I., 2005, ApJ, 634, 968
Bergin E. A., 2013, in Roig F., Pereira C. B., Alcaniz J. S., Daflon S. de la Reza R., eds, AIP Conf. Proc. Vol. 1638, XVII Special Courses at the National Observatory of Rio de Janeiro. Am. Inst. Phys., New York, p. 5
Blake G. A., Masson C. R., Phillips T. G., Sutton E. C., 1986, ApJS, 60, 357
Busquet G. et al., 2014, A&A, 561, 120
Caselli P., Ceccarelli C., 2012, A&AR, 20, 56
Cazaux S., Tielens A. G. G. M., Ceccarelli C., Castets A., Wakelam V., Caux E., Parise B., Teyssier D., 2003, ApJ, 593, L51
Ceccarelli C. et al., 2010, A&A, 521, L22
Charnley S. B., 2004, Adv. Space Res., 33, 23
Charnley S. B., Tielens A. G. G. M., Millar T. J., 1992, ApJ, 399, L71
Codella C. et al., 2009, A&A, 507, L25
Codella C. et al., 2012, ApJ, 757, L9
Fontani F., Codella C., Ceccarelli C., Lefloch B., Viti S., Benedettini M., 2014, ApJ, 788, L43
Garrod R. T., Herbst E., 2006, A&A, 457, 927
Gueth F., Guilloteau S., Bachiller R., 1996, A&A, 307, 891
Gueth F., Guilloteau S., Bachiller R., 1998, A&A, 333, 287
Herbst E., van Dishoeck E. F., 2009, ARA&A, 47, 427
Jaber A. A., Ceccarelli C., Kahane C., Caux E., 2014, ApJ, 791, 29
Lefloch B. et al., 2012, ApJ, 757, L25
Maret S., Hily-Blant P., Pety J., Bardeau S., Reynier E., 2011, A&A, 526, A47
Mendoza E., Lefloch B., López-Sepulcre A., Ceccarelli C., Codella C., Boechat-Robertry H. M., Bachiller R., 2014, MNRAS, 445, 151
Öberg K. I., Bottinelli S., Jørgensen J. K., van Dishoeck E. F., 2010, ApJ, 716, 825
Pickett H. M., Poynter R. L., Cohen E. A., Delitsky M. L., Pearson J. C., Müller H. S. P., 1998, J. Quant. Spectrosc. Radiat. Transfer, 60, 883
Podio L., Lefloch B., Ceccarelli C., Codella C., Bachiller R., 2014, A&A, 565, 64
Rawlings J. M. C., Williams D. A., Viti S., Cecchi-Pestellini C., 2013, MNRAS, 430, 264
Requena-Torres M. A., Martín-Pintado J., Rodríguez-Franco A., Martín S., Rodríguez-Fernández N. J., de Vicente P., 2006, A&A, 455, 971
Sakai N., Shirley Y. L., Sakai T., Hirota T., Watanabe Y., Yamamoto S., 2012, ApJ, 758, L4
Taquet V., Ceccarelli C., Kahane C., 2012, ApJ, 784, L3
Vastel C., Ceccarelli C., Lefloch B., Bachiller R., 2014, ApJ, 795, L2
Vasyunin A. I., Herbst E., 2013, ApJ, 769, 34

This paper has been typeset from a TEX/LATEX file prepared by the author.